Concentration Dependent Luminescence of Tb^{3+} ions in high Calcium-Alumino-Silicate Glasses

Atul D. Sontakke, Kaushik Biswas, K. Annapurna*

Glass Technology Laboratory, Central Glass and Ceramic Research Institute
(Council of Scientific and Industrial Research)
196, Raja S.C. Mullick Road, Kolkata 700032, India

Abstract

This study deals with the results on the concentration dependent fluorescence properties of Tb^{3+}-doped calcium aluminosilicate (CAS) glasses of composition (100-x)(58SiO_2-23CaO-5Al_2O_3-4MgO-10NaF in mol%)-x Tb_2O_3 (x = 0, 0.25, 0.5, 1, 2, 4, 8, 16, 24, 32, 40 in wt%). The FTIR reflectance spectra suggested the role of dopant ions as network modifiers in the glass network. The fluorescence spectra of low Tb^{3+}-doped glasses have revealed prominent blue and green emissions from $^5D_3$ and $^5D_4$ excited levels to ^7F_j ground state multiplet respectively. The glass with 2 wt% of Tb_2O_3 has exhibited maximum intensity of blue emission from $^5D_3$ level, while green emission from $^5D_4$ level has increased linearly up to 24 wt% and showed reduction in the rate of increase for higher Tb_2O_3 concentrations. The concentration quenching of blue emission ($^5D_3 \rightarrow {}^7F_j$) is attributed mainly to the resonant energy transfer (RET) assisted cross-relaxation (CR) among the excited and nearest neighbour unexcited Tb^{3+} ions in the glass matrix. The decline in rate of increase of green emission ($^5D_4 \rightarrow {}^7F_j$) at higher concentrations has been explained due to a possible occurrence of cooperative energy transfers leading to $4f^8 \rightarrow 4f^7 5d$ transition interactions. The blue and green emission decay kinetics have been recorded to compute the excited level ($^5D_3$ and $^5D_4$) lifetimes, which confirmed the Tb^{3+} concentration quenching of the blue emission in these glasses.

Key words: Calcium aluminosilicate glasses, Tb^{3+} green luminescence, concentration quenching

PACS : 32.50.+d; 42.70._a; 78.40._q ; 78.55.Qr

* Corresponding author : Tel.: +91-33 2473 3469; Fax: +91-33 2473 0957
Email : glasslab42@hotmail.com (K. Annapurna)

1. Introduction

Glasses doped with rare earth ions have achieved a great deal of interest for applications in optoelectronic devices such as solid-state lasers, channel waveguides and optical fibre amplifiers for optical communications. Although much of the current efforts have been focussed at the telecommunication window of 1.55 μm to 1.3 μm, the visible wavelength range could be of more interest for several applications, including optical data storage, display devices, laser material spectroscopy and biomedical spectroscopy. In addition, the rare earth ions in vitreous hosts, experience a variety of crystal fields due to lack of long-range order unlike crystalline materials. Among the rare earths, Tb^{3+} ions in different hosts could show an intense green emission and hence those have been used in the development of efficient green emitting phosphors and scintillator materials [1, 2]. Several reports have also confirmed the use of Tb^{3+} as an active ion in laser glasses [3, 4].

In recent years, a variety of glass systems based on heavy metal oxides (HMO), halides or chalcogenides have been investigated for low phonon energy hosts. But until now silicate based glass systems are of prime importance in term of commercialisation for practical applications. Among them, after soda-lime-silicate and borosilicate glasses, aluminosilicate glasses are considered to be attracting a great deal of scientific and industrial importance because of their good optical, thermal and mechanical properties. Due to their good mechanical properties, these aluminosilicate glasses are widely used in the manufacture of glass fibres such as E-glass and S-glass, which finds applications in fibre reinforced plastics and thermal insulating goods. The aluminosilicate glasses containing relatively high alumina without boric oxide are

found to be extremely resistive to alkali. As these glasses are having low density, moderately high modulus, high thermal expansion and capability of yielding good optically polished surfaces, they can be used as promising materials for information recording medium in the form of hard disc substrates [5].

In silicate networks, on introduction of network intermediates [Al^{3+}] and network modifier [Ca^{2+}] ions, the glass structure changes with the formation of some non-bridging oxygen (NBO's). The presence of the network modifiers such as Na^{+}, Mg^{2+} and Ca^{2+} could lead to the softening of the glass network. Such a kind of structure allows for an easy incorporation of rare earth ions without forming a large number of clusters, thereby resulting in a better statistical distribution of the dopant ions [6]. This suggests that the calcium aluminosilicate glass system could be a good host for rare earth ions. Similarly, Bettinelli et al. [7] have investigated the use of calcium sodium aluminosilicate glasses for optical fibre amplifiers. Also, the calcium aluminosilicate glasses are reported to be good host for visible upconversion and NIR lasing when doped with Er^{3+} or Nd^{3+} ions respectively [8, 9]. In addition to these, rare earth doped calcium aluminosilicate glasses and ceramic compounds have been extensively studied for their long lasting phosphorescence (LLP) properties due to their excellent energy storage capacity on irradiation causing 'defect centres' and later, efficient emission from them with a suitable excitation as a result of recombination [10]. As the alkaline earth aluminosilicate glasses possess wide band gap energies around 5.0 eV making them as suitable host materials to study $4f^n \rightarrow 4f^{n-1}5d$ transition interactions in dopant rare earth ions.

Hence, in the present work, high calcium aluminosilicate glasses of the chemical composition of (mol%) $58SiO_2$-$23CaO$-$5Al_2O_3$-$4MgO$-$10NaF$ doped with Tb_2O_3 in a varied concentrations in the range of 0.25, 0.5, 1.0, 2.0, 4.0, 8.0, 16.0, 24.0, 32.0, and 40.0 wt% have been considered to investigate concentration effect on its luminescence properties. The photoluminescence emission, excitation and decay behaviours of different Tb^{3+}-doped glasses have been analysed in terms of energy transfer mechanisms among the active ions and also by $4f^n \rightarrow 4f^{n-1}5d$ transition interactions. The UV-visible-NIR absorption and FTIR reflectance measurements of Tb^{3+}: CAS glasses have also been carried out to elicit the effect of Tb^{3+} ions concentration.

2. Experimental Studies

The glasses in the following chemical compositions (100-x)($58SiO_2$-$23CaO$-$5Al_2O_3$-$4MgO$-$10NaF$ in mol%)-x Tb_2O_3 (where x = 0, 0.25, 0.5, 1, 2, 4, 8, 16, 24, 32, 40 in wt%) were synthesized by a melt quenching method. Each 25 gm of homogeneously mixed batches were melted in pure platinum crucible at 1600^0C for an hour and later poured onto the iron mold that was preheated at 590^0C. Thus obtained glasses were annealed at 590^0C to relieve thermal stresses and cooled slowly to the room temperature using a precision temperature controlled annealing furnace. For further increase (>40 wt%) of dopant concentration in the chemical composition, we observed white mass at the bottom of the crucible. The host glass without dopant ion was also prepared as a reference. The prepared glass samples were cut and polished to 2 mm thick plates for optical measurements.

The density of Tb^{3+}-doped calcium aluminosilicate glasses was measured by Archimedes' method using water as buoyancy liquid. The refractive indices of all the glasses at different wavelengths were measured using Prism Coupler Technique on Metricon 2010/M Refractometer equipped with 473 nm, 532 nm, 632.8 nm and 1552 nm Lasers. The experimental refractive indices at four different wavelengths presented in Table 2 were fitted to Cauchy's relation [11] to obtain n_e, $n_{F'}$, and $n_{C'}$ at 546.1 nm, 480 nm and 653.8 nm wavelengths respectively in order to estimate the dispersion properties of all glasses.

The powder X-ray diffraction analysis was carried out on a Philips PW1710 diffractometer to confirm the vitreous nature of samples prepared. The FTIR reflectance spectra of different Tb^{3+}-doped glasses were obtained from Perkin-Elmer FTIR spectrophotometer (1615 series) attached with reflectance measurement arrangement with incident and reflectance angles set at 15^0. NIR absorption spectra measurement of different Tb^{3+}-doped glasses was carried out with the same FTIR spectrophotometer. The optical absorption spectra in UV-visible region were recorded on Shimadzu MPC3101 UV-VIS-NIR spectrophotometer in the range of 200 nm-600 nm with a resolution of 0.5 nm.

The photoluminescence (PL), excitation and decay curves measurements of different Tb^{3+}-doped glasses were recorded on SPEX spectrofluorimeter of model: Fluorolog-2. The steady state PL was measured using a 150 W continuous Xe lamp as the excitation source and fluorescence decay kinetics were recorded on the same

fluorimeter employed with 1934D phosphorimeter setup using pulsed 50 W Xenon lamp as the excitation source.

3. Results and Discussion

3.1 Physical and Non-linear optical properties

Table 1 presents some of the important physical properties of Tb^{3+}-doped calcium aluminosilicate glasses. The density (d) and average molecular weight (M_{avg}) of glasses are found to be increasing with the Tb^{3+} contents, which may be due to the incorporation of heavy metal (Tb^{3+}) ions in the glass network. Using the values of d and M_{avg}, the rare earth ion concentration (N_{Tb}) and three other parameters such as inter-ionic distances (r_i), polaron radius (r_p) and field strength (F) have been calculated using the standard formulae [12,13]. The optical properties such as Abbe number (ν_e), Molar refraction (R_M), Reflection loss (R%) and non-linear optical parameters such as n_2, γ and $\chi_{1111}^{(3)}$ have been evaluated from linear refractive indices n_e, $n_{F'}$ and $n_{C'}$ at wavelengths 546 nm, 480 nm and 643.8 nm respectively using relevant expressions [14-16] and the data is given in Table 3. The increase in the refractive indices of glasses with an increase in Tb^{3+} concentration is in accordance with the density. From this Table, it can be seen that Abbe number is decreasing from 60 to 50 with the Tb^{3+} concentration from Tb0.25 to Tb40 glasses which indicates the increase in mean dispersion due to Tb^{3+} ions presence in the glass matrix. The non-linear optical properties are also varying with Tb^{3+} content following the Abbe number. Although there is a decreasing trend noticed in Abbe number values, all

glasses in the present work possess the Abbe number above 50, which clearly indicates their potential as good laser host glasses [17].

3.2 Structural Analysis

The XRD patterns of the prepared glasses have revealed a broad peak with no specific pattern confirming their amorphous nature. The measured X-ray Diffractograms of Tb0.5 and Tb24 glasses are shown in Fig.1a as a specimen profile. On close examination of these profiles, it can be noticed that, there is a slight sharpening of the broad peak with an increase in Tb^{3+} concentration in the glasses signifying the structural changes. The structural change evaluation has been carried out for these glasses using FTIR reflectance spectroscopy as a tool. Fig.1b represents the recorded FTIR reflectance spectra of all Tb^{3+} glasses. The most intense reflectance band at around 1037 cm^{-1} may be attributed to the asymmetric stretching vibration modes of Si–O bond involving bridging oxygen {marked as [Si-O-Si] in the figure} and a shoulder at 938 cm^{-1} is due to the asymmetric stretching vibrations of Si–O bond involving non-bridging oxygen atoms {marked as [$Si-O^-$] in the figure} of SiO_4 tetrahedra [18,19]. The stretching vibration modes of [Al^{IV}-O-Al^{IV}] are detected around 724 cm^{-1} [20] which may be overlapped with two more weak bands originated from inter-tetrahedral [Si-O-Si] vibrations around 600-800 cm^{-1} [21]. The reflectance band at 462 cm^{-1} can be attributed to the bending modes of the Si-O bonds of SiO_4 tetrahedra [20]. For low Tb^{3+} concentration glasses, a weak band around 1149 cm^{-1} can be found which is attributed to the vibration modes of Si–O bond associated with [SiO_4] polymerized unit [22].

It is clearly seen from this figure that, the band related to asymmetric stretching vibration mode of [Si-O-Si] is found to be shifting towards lower energy from 1037 cm^{-1} to 1005 cm^{-1} with an increase in Tb^{3+} content, which may be due to the Tb^{3+} ions entering in glass matrix as network modifiers. The Tb^{3+} ions in the glass network are known to replace Ca^{2+} by increasing the non-bonding oxygen atoms (NBO's) and which decrease the degree of polymerisation [23]. So, the vanishing of band around 1149 cm^{-1} due to vibrations of [Si-O-Si] polymerisation units and strengthening of [$Si-O^{-}$] band at 938 cm^{-1} indicates the increase in NBOs with the decreasing silicate polymerised network on Tb^{3+} inclusion in the glass matrix. Yet another observation has also been made from FT-IR reflectance spectra is that there is a gradual broadening of band at 462 cm^{-1} of Si-O bending mode with a little shifting towards the higher energy side with an increase of the Tb^{3+} contents. This may be due to the contribution from Tb-O bond vibration, which is overlapping with Si-O bending vibration in Tb^{3+}-doped calcium aluminosilicate glasses. Overall analysis of FT-IR reflectance spectra demonstrate that, Tb^{3+} ions are entering into the calcium aluminosilicate glass as network modifiers.

3.3 Spectral analysis

3.3.1 Optical absorption spectra

The room temperature optical absorption spectra of different Tb^{3+}-doped calcium aluminosilicate glasses in UV-visible and Near Infrared wavelength range are shown in Fig. 2 (a, b) respectively. The spectra comprise of in-homogeneously broadened bands originating from $f \rightarrow f$ and $f \rightarrow d$ electronic transitions of magnetic and

electric dipole mechanisms in $4f^8$ and $4f^7 5d^1$ configuration of Tb^{3+} ions. In the spectra, recorded UV-VIS absorption peaks centred at 485 nm, 378 nm, 369 nm, 352 nm, 338 nm and 317 nm have been assigned to the transitions from ground state $^7F_6$ to the higher excited levels of $^5D_4$, ($^5D_3$, $^5G_6$), $^5L_{10}$, ($^5L_9$, $^5G_4$), ($^5G_2$, $^5L_6$) and ($^5H_7$, $^5D_{0,\ 1}$) respectively of $4f^8$ configuration and an absorption band around 299 nm may be due to the $4f^8 \rightarrow 4f^7 5d^1$ transition of Tb^{3+} ions [24-26]. In NIR region (Fig.2b), the detected absorption bands at wavenumbers 2384 cm^{-1}, 3567 cm^{-1}, 4590 cm^{-1}, 5123 cm^{-1}, 5272 cm^{-1} and 5557 cm^{-1} are arising due to transitions within ground state multiplets $^7F_6 \rightarrow$ $^7F_5$, $^7F_4$, $^7F_3$, $^7F_2$, $^7F_1$ and $^7F_0$ levels respectively. In concurrence with the partial energy level diagram as shown in Fig.7, the observed energy separation of ground state mulitiplets (^7F_j level) decreasing from $^7F_6$ to $^7F_0$ level.

It is clear from Fig.2a that the UV cut-off edge is shifting towards higher wavelength with the increase of Tb^{3+} concentration. This red shift of the UV edge has resulted in a pale yellow coloured tint in the glasses with higher Tb^{3+} concentration. By using the conventional Mott-Davis equation [27], the allowed direct and indirect band gap energies (E_g) of these glasses have been estimated and presented in Table 4. From this data it can be seen that the band gap energy of reference glass is found to be 5.3 eV and its value is decreasing gradually as a function of Tb^{3+} addition in the glasses. The probable transitions responsible for this shift of UV cut-off edge have been observed clearly from the excitation spectra (Fig.3) of these glasses.

3.3.2 Excitation and Fluorescence spectra

Fig.3 shows the excitation spectra of different Tb^{3+}-doped calcium aluminosilicate glasses by monitoring the green emission of Tb^{3+} at 545 nm. For a clear understanding, the overall excitation spectrum can be divided into two parts. One, in the wavelength range 220 nm-310 nm comprises of $4f^8 \rightarrow 4f^7 5d^1$ transitions and other part of the excitation spectrum, in the range 310 nm–500 nm stands for $4f^8$-$4f^8$ transitions of the Tb^{3+} ions [26]. In the case of Tb^{3+} (n>7), not all transitions between $4f^8$ and $4f^7 5d$ levels are allowed. According to energy level coupling schemes, $4f^8 \rightarrow 4f^7 5d^1$ allowed transitions (denoted as $^7D_{5,\ 4,\ 3,\ 2,\ 1}$ multiplets) occur when *5d* electrons are anti-parallel spin with respect to the total spin and they would appear as first highest energy peaks and spin forbidden transitions (represented as $^9D_{6,\ 5,\ 4,\ 3,\ 2}$ multiplets) result in when *5d* electrons are parallel with respect to the total spin [28]. Thus in the excitation spectra of present glasses, the first band around 244 nm and another at 284 nm can be assigned to the spin allowed ^7D and spin forbidden ^9D levels of $4f^8 \rightarrow 4f^7 5d$ transitions of Tb^{3+} ions respectively [29,30]. Both these transitions have been detected as a single broad band with clear Stark components as has been depicted in the inset of Fig. 3. It could be noticed from this figure that at the lower concentrations of Tb^{3+} up to 2 wt%, the intensity of peak at 244 nm representing ^7D_j spin allowed transitions has been found to be more compared to the intensity of ^9D_j spin forbidden multiplet transitions at 284 nm but this relative intensity has been reversed with the increase of terbium concentration beyond 2 wt% in glass samples. This behaviour of excitation band intensities implies an important interaction between the high spin *5d* levels and the excited energy levels of $4f^8$ configuration of Tb^{3+} ions [31], which will be discussed later.

The second part of the excitation spectra of Tb^{3+} calcium aluminosilicate glasses has demonstrated two intense peaks of $f-f$ transitions, i) a broad band centred at 374 nm and it is attributed to superimposition of transitions $^7F_6 \rightarrow (^5D_3, {}^5G_6)$, $^5L_{10}$, $(^5L_9, {}^5G_4)$, $(^5G_2, {}^5L_6)$ and $(^5H_7, {}^5D_{0,\ 1})$ respectively [24, 25] and ii) at 482 nm is assigned to transition $^7F_6 \rightarrow {}^5D_4$. All these excitation transitions are analogous to those observed in optical absorption spectra (Fig.2a). The excitation band at 374 nm has not been resolved fully due to the fact that energy levels lay above $^5D_3$ level are all very closely spaced as shown in the partial energy level diagram (Fig.7). Another noticeable feature of the excitation spectra of studied Tb^{3+}-doped glasses is that, the variation of relative intensities of excitation peaks due to transitions $^7F_6 \rightarrow {}^5D_3$ (374 nm) and $^7F_6 \rightarrow {}^5D_4$ (482 nm) as a function of Tb^{3+} concentration. For the glasses from Tb0.25 up to Tb1, excitation peak at 482 nm is more intense than the peak at 374 nm, but with the increase of Tb^{3+} concentration, the excitation intensity of $^7F_6 \rightarrow {}^5D_3$ transition has exhibited its dominance in intensity. This could be correlated to the percentage contribution of these two levels ($^5D_3$ and $^5D_4$) to the fluorescence characteristics of Tb^{3+} doped glasses with the concentration variation of dopant ions.

Fig. 4 shows the fluorescence (Photoluminescence) spectra of different Tb^{3+}-doped calcium aluminosilicate glasses excited to $^5D_3$ level (374 nm). The fluorescence spectra demonstrated the emission transitions arising from both $^5D_3$ and $^5D_4$ energy levels to ^7F_j ground state multiplets. The emission peaks at 418 nm, 438 nm and 460 nm have been attributed to $^5D_3 \rightarrow {}^7F_{5,\ 4,\ 3}$ transitions and those located at 490 nm, 545 nm, 586 nm, 625 nm, 660 nm, 675 nm and 687 nm have been ascribed to $^5D_4 \rightarrow {}^7F_{6,\ 5,\ 4,\ 3,\ 2,\ 1,\ 0}$ transitions respectively. The intensity variation of blue ($^5D_3 \rightarrow {}^7F_4$ at 438 nm)

and green ($^5D_4 \rightarrow {}^7F_5$ at 545 nm) emissions as a function of Tb^{3+} ions concentration has been graphically represented in Fig. 5. It is observed from Figs.4 and 5 that the $^5D_3$ emission intensity of Tb^{3+} ions increases initially for Tb0.25 up to Tb2 glass and then decreased for all other glasses in the series with increase of concentration, but the intensity of green emission from $^5D_4$ level has shown a linear increase with Tb^{3+} ions concentration up to 24 wt% and its rate of increase was slowed down for further rise in concentration. The change of green emission intensity I($^5D_4 \rightarrow {}^7F_5$) with respect to blue emission I($^5D_3 \rightarrow {}^7F_4$) as a function of Tb^{3+} ions concentration has been presented in Fig.6 for clear understanding. The curve showed three distinct zones of green to blue relative emission intensity ($I_{G/B}$) variation. In the first zone, there is a slow increase for the glasses Tb0.25 up to Tb2 followed by a rapid increase in the second zone of Tb2 to Tb24 glasses and again exhibiting a slow increase in the third portion of the curve which comprises of Tb24-Tb40 glasses. This trend implies that, the intensity of emission transitions from $^5D_3$ is quite comparable to that from $^5D_4$ level at low Tb^{3+} concentration (Tb0.25-Tb2 glasses) that is accompanied by a decrease in $^5D_3$ emission intensity with an increase of emission from $^5D_4$ level in glasses Tb4-Tb24 and later further bending of curve for Tb32 to Tb40 glasses may be because of a reduced rate of increase in $^5D_4$ emission. This may be due to the concentration quenching of the $^5D_3$ emission, which becomes more prominent for higher Tb^{3+} ion concentration because of the reduction in the inter ionic distances. That is why; the excitation band at 374 nm is relatively stronger than 482 nm band for higher Tb^{3+} ion concentrations, contributing more to $^5D_4$ emission by cascading relaxation of $^5D_3$ level population. Thus in the investigated calcium aluminosilicate host 2 wt% Tb_2O_3 is found to be the optimum concentration for a strong emission from $^5D_3$ level.

Generally in any host, the non-radiative processes such as multi-phonon decay, quenching by impurities and energy migration among active ions are mainly responsible for the quenching of dopant luminescence efficiency. In the present calcium aluminosilicate glass host, the highest lattice phonon energy is found to be around 1030 cm^{-1} [32], which reflects the fact that it needs at least five phonons to bridge the energy gap (5990 cm^{-1}) of $^5D_3$ - $^5D_4$ levels and more than fifteen phonons to depopulate $^5D_4$ level to its lower ground state energy levels as the energy gap of $^5D_4$ - ^7F_j is more than 15000 cm^{-1}, hence the multi-phonon decay can be neglected in the later case. The hydroxyl ion (OH^-) impurity in glasses acts as high-energy phonons (~3000 cm^{-1}), which may cause rapid quenching of $^5D_3$ energy levels of the Tb^{3+}ions. But in all Tb^{3+} doped glasses prepared under this study, the OH^- ion content has been estimated from FT-IR absorption spectrum (not shown) using standard procedure is found to be 34 ppm [33], whose influence is expected insignificant on the quenching of fluorescence intensity. Although, there is possibility of multi-phonon assisted non-radiative relaxation of $^5D_3$ to $^5D_4$ level due to its low energy gap around 5990 cm^{-1}, at low concentrations, but this could be dominated by a faster cross relaxation (CR) phenomenon due to a resonance energy transfer (RET) through $^5D_3 \rightarrow {}^5D_4 \Rightarrow {}^7F_6 \rightarrow {}^7F_0$ process as the energy difference between $^5D_3$ and $^5D_4$ matches well with the energy gap between $^7F_6$ and $^7F_0$ energy levels [29] as shown in Fig. 7 which becomes more prominent at higher Tb^{3+} ion concentrations.

Choi et al. [29] and Sohn et al. [34] have suggested a second type of quenching mechanism for $^5D_3$ and $^5D_4$ excited levels based on the excited state absorption by a cooperative energy transfer from $^5D_3$ or $^5D_4$ levels to the upper laying levels (UL). According to them, this process has been proposed as in three possible ways such as

(i) $^5D_4 \rightarrow {}^7F_6 \Rightarrow {}^5D_4 \rightarrow UL$; (ii) $^5D_4 \rightarrow {}^7F_6 \Rightarrow {}^5D_3 \rightarrow UL$ and (iii) $^5D_3 \rightarrow {}^7F_6 \Rightarrow {}^5D_3 \rightarrow UL$

For these to occur, at least two excited active ions need to be in close vicinity of each other, so that by de-exciting one, other can jump to the upper levels such as ^7D, ^9D of $4f^7 5d^1$ configuration or CTB and some times to the host absorption band (HAB).

As the cross relaxation by resonance energy transfer occurs among the excited active ions and its nearest neighbouring unexcited active ions, it is more probable for active ions to be surrounded with unexcited ions than the excited ions. Hence, it may be said that the cross relaxation mechanism contributes more to $^5D_3$ quenching than cooperative energy transfer to upper levels. While in the case of $^5D_4$ excited level, non-radiative relaxation is a slow mechanism and it observed to occur in glasses at higher concentration of terbium such as Tb24 and above which has been discussed earlier in this section. As there is no cross relaxation mechanism for $^5D_4$ quenching, only energy migration among excited state active ions leading to upper level interactions is the possible route. At higher concentration, more excited ions may be closer to each other, which is clear from the estimated values of critical distance (R_0) and energy transfer parameter (W_{tr}) listed out in Table 5. In addition, the $^5D_4 \rightarrow {}^7F_j$ transitions are in near resonance with the transitions of $^5D_4 \rightarrow {}^7D$ or ^9D bands of $4f^7 5d^1$ configuration of Tb^{3+} ion. So it may assumed that, $^5D_4$:$^5D_4 \rightarrow {}^7F_6$:Upper Levels cooperative energy transfer mechanism is the main quenching mechanism for $^5D_4$ excited level emission rate decrease above Tb24 and subsequent quenching for higher concentration. This fact has also been substantiated by the relative intensity changes exhibited by the observed $4f^8 \rightarrow 4f^7 5d$ transitions in the higher energy portion of excitation spectra (inset of Fig 3) of Tb^{3+} doped calcium aluminosilicate glasses.

From the inset of Fig. 3 it is clear that the intensity of spin forbidden ^9D transitions increased over the allowed ^7D transitions, which may be due to possible occurrence of $4f^8$- $4f^7 5d$ level interactions.

3.3.3 Fluorescence Decay analysis

Fluorescence decay analysis is very useful for understanding the energy transfer mechanism and quenching behaviour of luminescence of Tb^{3+} ions. The Fig. 8 and Fig. 9 show the fluorescence decay curves for $^5D_3 \rightarrow {}^7F_4$ (at 438 nm) and $^5D_4 \rightarrow {}^7F_5$ (at 545 nm) emission transitions respectively. Table 5 presents the values of measured decay times (τ_m). From Fig. 8, it is observed that, the decay curve for Tb0.25 glass is in single exponential. So, it can be assumed that there is no energy transfer induced quenching for Tb0.25 glass and the decay time can be treated as intrinsic single-ion lifetime for Tb^{3+} ions in this host. For further increase in Tb^{3+} concentration, the decay curves begin to show non-exponentiality and it becomes more prominent. This deviation from the exponential behaviour and decrease in the decay time (Table 5) is attributed to the radiation less process due to the energy transfer among active ions, either due to cross-relaxation or the cooperative energy transfer to upper levels. In the present glass system it is assumed that, the quenching of blue fluorescence ($^5D_3 \rightarrow {}^7F_j$) is caused by cross relaxation and reduction of green emission ($^5D_4 \rightarrow {}^7F_j$) intensity at higher concentration is due to the cooperative energy transfer to upper levels. For $^5D_3 \rightarrow {}^5D_4$ cross-relaxation, it is possible to obtain the critical distance R_0 from the concentration quenching data. R_0 is the critical separation between donor and acceptor, at which the non-radiative rate equals to that of the

radiative rate for the internal single ion relaxation [29]. The radiative rate of $^5D_3$ emission for Tb^{3+} ions in Tb0.25 glass is found to be 584 s^{-1}. In addition to this, the critical concentration, which is defined as the concentration at which observed decay time (τ_{obs}) decreases to the half value of intrinsic decay time ($\tau_{intrinsic}$) because non-radiative decay rate ($1/\tau_{non}$) equals to $1/\tau_{intrinsic}$ at this concentration. From these, the critical concentration and critical distance have been estimated to be approximately little less than 2 wt% (Tb2 glass) and about 12 Å respectively following the Hirayama-Inokuti relation [35]. Table 5 also lists the values of derived energy transfer rate (W_{tr}) and energy transfer efficiency (η_{tr}) obtained from the relevant relations [36]. From this table it is clear that, the energy transfer efficiency is almost 50% for Tb2 glass confirming the 2 wt% Tb_2O_3 is the critical concentration and corresponding separation is the critical distance for the $^5D_3$ blue emission quenching.

Further, the non-exponential behaviour of the decay curve has been fitted using Hirayama-Inokuti model based on the conventional energy transfer mechanisms involving multipole interactions [37]. Following this model, in order to fit the decay curves, the exact nature of the interaction involved in the energy transfer is to be known. The plot depicted in Fig. 10 of $\ln[-\ln(I(t)/I_0)-(t/\tau_0)]$ vs. $\ln(t/\tau_0)^3$ gives the slope equals to 1/s, where s is the fitting parameter that determines the nature of the electric multipole interactions involved. The value of s estimated from the slope is found to be in the range 5 - 6 indicating the dipole-dipole interactions may be responsible for the energy transfer [35]. The critical distance (R_0) calculated using Hirayama-Inokuti fitting is 9.03 Å, which is in agreement with that of the calculated value 12 Å as

described above. Fig. 11 represents the variation of decay times of $^5D_3$ and $^5D_4$ levels with the increase of Tb^{3+} ion concentration.

The reduction in rate of increase of green emission from $^5D_4$ level may be mainly due to second type of quenching mechanism through cooperative energy transfer to upper *5d* levels, resulting in the non-linearity of decay curves and decrease in lifetime of $^5D_4$ at higher concentrations of terbium. However, there is no overall quenching of green emission ($^5D_4 \rightarrow {}^7F_j$) within the concentration range studied in the present glass system.

4. Conclusions

In summary, it could be concluded that a series of calcium aluminosilicate (CAS) optical glasses in the chemical composition (100-x) ($58SiO_2$-$23CaO$-$5Al_2O_3$-$4MgO$-10NaF in mol%)-x Tb_2O_3 (x = 0, 0.25, 0.5, 1, 2, 4, 8, 16, 24, 32, 40 in wt %) have successfully been prepared by a melt quenching technique. The 40 wt% of dopant ion concentration was found to be maximum concentration for its dissolution in the melt. The following important conclusions could be drawn based on the results concerning the glasses through their FT-IR Reflectance Spectra, UV-VIS-NIR absorption, fluorescence excitation, emission and decay kinetics measurements:

a) The FTIR reflectance spectra of different Tb^{3+}-doped glasses have clearly demonstrated structural changes with the addition of Tb_2O_3 content in the glass network, which indicates the functioning of the dopant ions as network modifier ions.

b) The optical absorption spectra in 250-550 nm wavelength range have revealed 4*f-4f* absorption transitions of $^7F_6 \rightarrow (^5D_3, {}^5G_6)$, $^5L_{10}$, $(^5L_9, {}^5G_4)$, $(^5G_2, {}^5L_6)$, $(^5H_7, {}^5D_{0,\ 1})$ and $^5D_4$ of $4f^8$ configuration and also *4f-5d* transitions at the band edge. The allowed direct band gap energies (E_g) of calcium aluminosilicate glass has been decreased from 5.3 eV of un-doped glass to 4.44 eV for 40 wt% Tb_2O_3 doped glass which is attributed to the *4f-5d* level interactions.

c) The photoluminescence (PL) spectra of low Tb^{3+}-doped glasses have shown prominent blue and green emissions from both $^5D_3$ and $^5D_4$ excited levels respectively. However, the intensity of blue emission has been found to be increasing for Tb_2O_3 concentration up to 2 wt% and decreasing for any further concentration increase. Despite an increase in $^5D_4$ level emission, this level also tends to show a decrease in its rate of increase of intensity for 32 wt% Tb_2O_3 concentration and beyond. The concentration quenching of the blue ($^5D_3 \rightarrow {}^7F_j$) emission has been attributed to the resonant energy transfer (RET) or cross-relaxation (CR) among the excited and nearest neighbour unexcited Tb^{3+} ions in the glass matrix. The slow increase of green emission at higher concentrations could be due to a possible occurrence of cooperative energy transfers to the upper laying *5d* bands among the excited state Tb^{3+} ions.

d) The critical distance (R_0) for $^5D_3$ quenching by a cross relaxation derived from Hirayama-Inokuti relation is found to be around 12 Å and the energy transfer coupling is attributed to the dipole-dipole interactions.

e) The fluorescence decay curves have shown single exponential decay features in the glasses at low Tb concentrations but those have shown non-exponential profiles at higher Tb_2O_3 concentrations due to non-radiative quenching of the

excited states. The estimated lifetimes of $^5D_3$ and $^5D_4$ levels are in the range of 1.71-0.08 ms and 3.38-2.44 ms, which are found to be decreasing with an increase of Tb^{3+} concentration.

Finally, it can be stated that there exists quite significant concentration quenching in the blue fluorescence ($^5D_3 \rightarrow {}^7F_j$) of Tb^{3+} ions doped calcium aluminosilicate glasses. However, there has not been overall quenching effect on the green emission ($^5D_4 \rightarrow {}^7F_j$) within the concentration range investigated for the glasses in the present work. Therefore, this Tb^{3+}-doped calcium aluminosilicate glass may be a promising host for green emission.

Acknowledgements

Authors would like to thank Dr. H. S. Maiti, Director, CGCRI for his kind encouragement and permission to publish this work. Our thanks are also due to Dr. Ranjan Sen, for his kind support in the present work. One of us (Mr.ADS) is thankful to the CGCRI, CSIR for the award of Research Internship to him.

References

[1] T. Welker, J. Lumin. 48, 49 (1991) 49.

[2] A. Vedda, M. Martini, M. Nikl, E. Mihokova, K. Nitsch, N. Solovieva and F. Karagulian, J. Phys.C: Condens. Mater. 14 (2002) 7417.

[3] T. Yamashita and Y. Ohishi, Electron. Lett. 43 (2007) 88.

[4] Gan Fuxi, 'Laser Materials', World Scientific Pub Co Inc. (1995).

[5] F. M. Behan and L. R. Pickney, USPTO application 20080130171.

[6] V. Petkov, S. J. L. Billing, D. S. Shastri and B. Himmel, Phys. Rev. Lett. 85 (2000) 3436.

[7] M. Bettinelli, M. Brenci, R. Dalligna, M. Ferrari, C. Mazzoleni, G.C. Righini and A. Speghini, Techna Srl Faenza (1999) 249.

[8] R. Naccache, F. Vetrone, J. C. Boyer, J.A. Capobianco, A. Speghini, M. Bettinelli and G.C. Righini, Mater. Lett. 58 (2004) 2207.

[9] D. F. de Sousa, L. A. O. Nunes, J. H. Rohling and M. L. Baesso, Appl. Phys. B: Lasers and optics 77 (2003) 59.

[10] Jianrong Qui, K. Miura, H. Inouye, Y. Kondo, T. Mitsuyu and K. Hirao, Appl. Phys. Lett. 73 (1998) 1763.

[11] F. A. Jenkins and H. E. White, Fundamentals of Optics, 4th Ed. McGraw Hill Inc. 1981.

[12] M. M. Ahmad, E. A. Hogarth and M. N. Khan, J. Mater. Sci. 19 (1984) 4041.

[13] A. J. Glass laser program annual report, Lawrence-Livermore Labs. Report No. URCL-50021-72 (1975).

[14] M. J. Weber, J. E. Lynch, D. H. Blackburn and D. T. Cronin, IEEE J. Quantum Electron 19 (1983) 1600.

[15] S. H. Kim, J. Yoko and S. Sakka, J. Am. Ceram. Soc. 76 (1993) 865.

[16] H. E. Rast, J. C. Fry and H. H. Casper, J. Chem. Phys. 46 (1967) 1460.

[17] N. L. Boling and A. J. Glass, IEEE J. Quantum Electron. 14 (1978) 601.

[18] X. Zhou, P. F. Johnson, R. A. Condrate Sr. and Y. M. Guo, Mater. Lett. 9 (1990) 207.

[19] M. E. Lynch, D. C. Folz and D. E. Clark, J. Non-Cryst. Solids 353 (2007) 2667.

[20] D. S. Wang and C. G. Pantano, J. Non-Cryst. Solids 142 (1992) 225.

[21] D. de Sausa Meneses, M. Malki and P. Echegut, J. Non-Cryst. Solids 352 (2006) 5301.

[22] D. E. Clark, E. C. Ethridge, M. F. Dilmore and L. L. Hench, Glass Technol. 18 (1977) 121.

[23] S. K. Lee and J. F. Stebbins, Geochim. Cosmochim. Acta 70 (2006) 4275.

[24] T. Yamashita and Y. Ohishi, J. Non-Cryst. Solids 354 (2008) 1883.

[25] K. Annapurna, R. N. Dwivedi, P. Kundu and S. Buddhudu J. Mater Sci. 39 (2005) 1051.

[26] Zhouyun Ren, Chunyan Tao, Hua Yang and Shouhua Feng, Mater. Lett. 61 (2007) 1654.

[27] N.F. Mott and E.A. Davis, Phil. Mag. 22 (1970) 903.

[28] P. Dorenbos, J. Lumin. 91 (2000) 91.

[29] Yoon Yang Choi, Kee-Sun Sohn, Hee Dong Park and Se Yong Choi, J. Mater. Res. 16 (2001) 881.

[30] Bing Yan, Hong-Hua Huang, J. Mater. Sci. 39 (2004) 3529.

[31] M. A. Gusowsky and W. Ryba-Romanowsky, Optics Lett. 33 (2008) 1786.

[32] M.L. Baesso, A.C. Bento, L.C.M. Miranda, D.F. de Souza, J. A. Sampaio, L.A.O. Nunes, J. Non-Cryst. Solids 276 (2006) 8.

[33] H. Ebendorff-Heidepriem, W. Seeber and D. Ehrt, J. Non-cryst. Solids 163 (1993) 74.

[34] Kee-Sun Sohn and Namsoo Shin, Electrochemical and Solid-State Lett. 5 (2002) H21-H23.

[35] J. K. Park, C. H. Kim, C. H. Han, H. D. Park, S. Y. Choi, Electrochem. Solid-State letters. 6 (2003) H13.

[36] M. Li, L. G. Reddy, R. Bennett, N. D. Silva, L. R. Jones, D. D. Thomas, Byophysical J. 76 (1999) 2587.

[37] M. Inokuti, F. Hirayama, J. Chem. Phys. 43 (1965) 1978.

Figure Captions

Fig. 1a: XRD pattern of Tb^{3+}: Calcium aluminosilicate glasses

Fig. 1b: FTIRRS of Tb^{3+}: Calcium aluminosilicate glasses

Fig. 2: UV-VIS (a) and NIR (b) Absorption spectra of Tb^{3+}: calcium aluminosilicate glasses

Fig. 3: Excitation spectra of Tb^{3+}-doped calcium aluminosilicate glasses

Fig. 4: Fluorescence spectra of Tb^{3+}-doped calcium aluminosilicate glasses (a) Tb0.25, (b) Tb0.5, (c) Tb1, (d) Tb2, (e) Tb4, (f) Tb8, (g) Tb16, (h) Tb24, (i) Tb32 and (j) Tb40

Fig. 5: Variation of Green ($^5D_4 \rightarrow {}^7F_5$) and Blue ($^5D_3 \rightarrow {}^7F_4$) emission intensity as a function of Tb^{3+} concentration in calcium aluminosilicate glasses

Fig. 6: Variation of Relative Fluorescence intensity ratio as a function of Tb^{3+} concentration in calcium aluminosilicate glasses

Fig. 7: Partial energy level diagram of Tb^{3+} ions in calcium aluminosilicate glasses

Fig. 8: Decay curves of luminescence transition ($^5D_3 \rightarrow {}^7F_4$) of Tb^{3+}: calcium aluminosilicate glasses (inset : semi-log plot)

Fig. 9: Decay curves of luminescence transition ($^5D_4 \rightarrow {}^7F_5$) of Tb^{3+}: calcium aluminosilicate glasses (inset : semi-log plot)

Fig. 10: Plots of experimental data $\ln(t/\tau_0)^3$ vs. $\ln[-\ln(I(t)/I_0)-(t/\tau_0)]$ of transition ($^5D_3 \rightarrow {}^7F_4$) with the solid lines representing theoretical fits.

Fig. 11: Variation of Decay time of $^5D_3$ and $^5D_4$ excited levels as a function of Tb^{3+} concentration in calcium aluminosilicate glasses

Table 1: Important physical properties, Glass average molecular weight (M_{avg}), Density (d), Terbium ion concentration (N_{Tb}), Interionic distance (r_i), Polaron radius (r_p) and Field strength (F) of Tb^{3+}-doped calcium aluminosilicate glasses.

Glass	**M_{avg} (g/mol)**	**d (g/cm^3)**	**N_{Tb} (10^{20} ions/cm^3)**	**r_i (Å)**	**r_p (Å)**	**F (10^{14} cm^{-2})**
Tb0	58.65	2.690	0	-	-	-
Tb0.25	59.77	2.694	0.217	35.86	14.45	1.44
Tb0.5	59.88	2.696	0.433	28.48	11.48	2.28
Tb1	60.15	2.708	0.865	22.61	9.11	3.61
Tb2	60.63	2.725	1.727	17.96	7.24	5.73
Tb4	61.60	2.776	3.448	14.27	5.75	9.07
Tb8	63.52	2.834	6.787	11.38	4.59	14.26
Tb16	67.28	2.964	13.21	9.11	3.67	22.26
Tb24	70.96	3.161	19.82	7.96	3.21	29.15
Tb32	74.55	3.270	25.71	7.30	2.94	34.67
Tb40	78.05	3.403	31.56	6.82	2.75	39.75

Table 2: Measured refractive indices (n) at 473 nm, 532 nm, 632.8 nm, 1552 nm wavelengths of Tb^{3+} doped and undoped calcium aluminosilicate glasses.

Glass	$\mathbf{n_{473}}$	$\mathbf{n_{532}}$	$\mathbf{n_{632.8}}$	$\mathbf{n_{1552}}$
Tb0	1.561	1.557	1.552	1.538
Tb0.25	1.564	1.559	1.555	1.540
Tb0.5	1.562	1.556	1.551	1.537
Tb1	1.564	1.559	1.554	1.540
Tb2	1.567	1.562	1.557	1.543
Tb4	1.571	1.566	1.560	1.545
Tb8	1.575	1.569	1.564	1.550
Tb16	1.585	1.581	1.576	1.559
Tb24	1.606	1.601	1.595	1.579
Tb32	1.616	1.609	1.604	1.588
Tb40	1.626	1.620	1.614	1.598

Table 3: Linear refractive indices (n_e (at λ=546.1nm), $n_{F'}$ (at λ=480nm), $n_{C'}$(at λ=653.8nm)), Abbe number (ν_e), Reflection loss (R%), Molar refractivity (R_M (cm^3)), non-linear refractive index (n_2 (10^{-13}esu)), non-linear refractive index coefficient (γ (10^{-16} cm^2/W)), and third order nonlinear susceptibility ($\chi_{1111}^{(3)}$ (10^{-15} esu)) of Tb^{3+}-doped calcium aluminosilicate glasses.

Glass	**Tb0**	**Tb0.25**	**Tb0.5**	**Tb1**	**Tb2**	**Tb4**	**Tb8**	**Tb16**	**Tb24**	**Tb32**	**Tb40**
n_e	1.556	1.559	1.555	1.559	1.562	1.565	1.569	1.581	1.600	1.609	1.619
$n_{F'}$	1.561	1.564	1.560	1.564	1.567	1.570	1.574	1.585	1.605	1.615	1.625
$n_{C'}$	1.551	1.554	1.550	1.554	1.556	1.559	1.563	1.574	1.594	1.603	1.613
ν_e	60.02	57.88	56.66	55.88	55.80	55.78	55.08	54.35	53.64	51.45	50.47
R %	4.73	4.77	4.72	4.77	4.81	4.85	4.91	5.06	5.32	5.45	5.59
R_M	7.14	7.17	7.13	7.17	7.21	7.23	7.34	7.56	7.68	7.89	8.05
n_2	1.43	1.52	1.56	1.60	1.62	1.64	1.69	1.78	1.92	2.10	2.22
γ	3.85	4.09	4.19	4.31	4.35	4.38	4.51	4.72	5.03	5.46	5.74
$\chi_{1111}^{(3)}$	5.90	6.30	6.42	6.63	6.72	6.80	7.03	7.47	8.15	8.92	9.54

Table 4: Optical bandgap energies (E_g^{opt}) of allowed direct and indirect transitions in Tb^{3+}-doped calcium aluminosilicate glasses.

Glass sample	Bandgap Energy, E_g^{opt} (eV)	
	Direct Transitions	**Indirect Transitions**
Tb0	5.30	4.78
Tb0.25	5.03	4.64
Tb0.5	4.94	4.54
Tb1	4.86	4.50
Tb2	4.81	4.47
Tb4	4.77	4.41
Tb8	4.71	4.35
Tb16	4.65	4.29
Tb24	4.54	4.17
Tb32	4.48	4.10
Tb40	4.45	4.05

Table 5: Measured Decay time (τ_m) for $^5D_3 \rightarrow {}^7F_4$, $^5D_4 \rightarrow {}^7F_5$ transitions, Energy transfer parameter (W_{tr}) and Energy transfer efficiency (η_{tr}) of Tb^{3+}-doped calcium aluminosilicate glasses.

Glass	**($^5D_3 \rightarrow {}^7F_4$) Transition**			**($^5D_4 \rightarrow {}^7F_5$) Transition**		
	τ_m (ms)	**W_{tr} (s^{-1})**	**η_{tr} (%)**	**τ_m (ms)**	**W_{tr} (s^{-1})**	**η_{tr} (%)**
Tb0.25	1.71	-	-	3.38	-	-
Tb0.5	1.37	146	19.88	3.38	-	-
Tb1	0.89	538	47.95	3.38	-	-
Tb2	0.83	617	51.46	3.05	32.2	9.76
Tb4	0.32	2539	81.28	2.98	40.3	11.83
Tb8	0.14	6461	91.81	2.83	57.0	6.27
Tb16	0.08	11565	95.32	2.63	83.9	22.19
Tb24	-	-	-	2.55	95.7	24.55
Tb32	-	-	-	2.48	106.9	26.63
Tb40	-	-	-	2.32	135.9	31.36

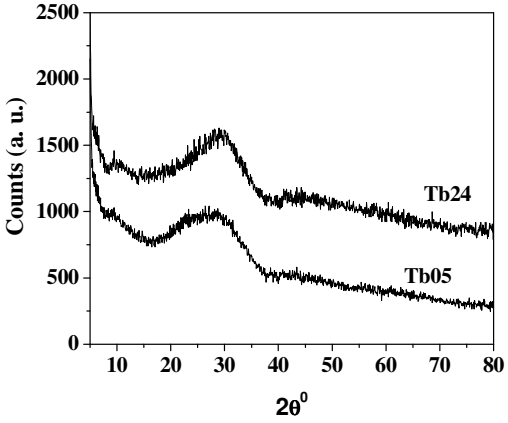
Counts (a. u.)
2θ0
Tb24
Tb05

Fig. 1(a)

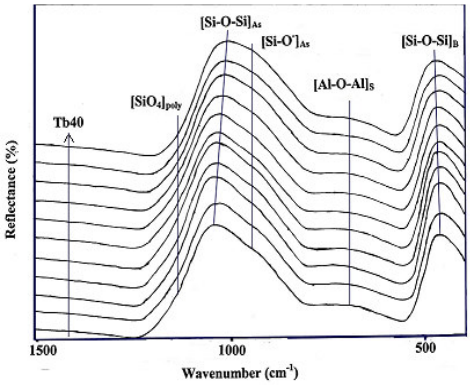
Reflectance (%)
Wavenumber (cm-1)
Tb40
[SiO4]poly
[Si-O-Si]As
[Si-O-]As
[Al-O-Al]S
[Si-O-Si]B

Fig. 1(b)

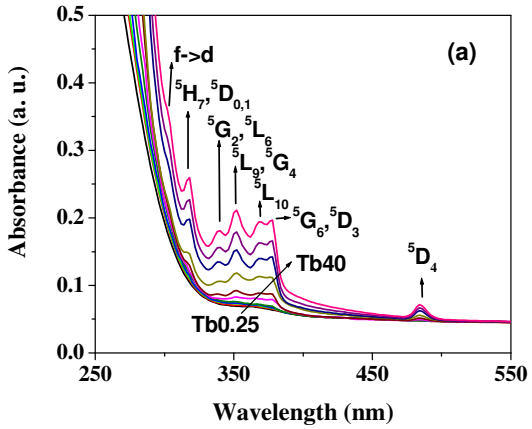
Absorbance (a. u.)
Wavelength (nm)
0.0
0.1
0.2
0.3
0.4
0.5
250
350
450
550
(a)
f->d
$^5H_7$, $^5D_{0,1}$
$^5G_2$, $^5L_6$
$^5L_9$, $^5G_4$
$^5L_{10}$
$^5G_6$, $^5D_3$
$^5D_4$
Tb40
Tb0.25

Fig. 2(a)

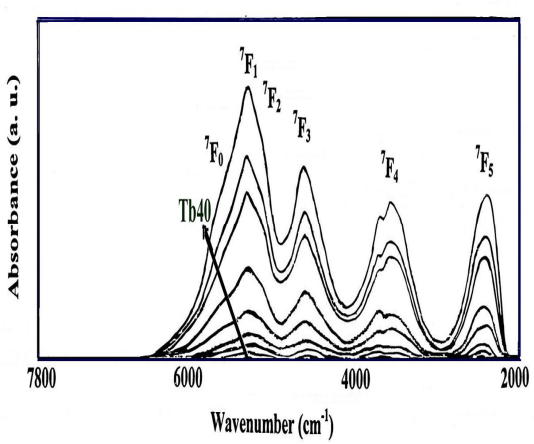
Absorbance (a. u.)
Wavenumber (cm^{-1})
7800
6000
4000
2000
$^7F_0$
$^7F_1$
$^7F_2$
$^7F_3$
$^7F_4$
$^7F_5$
Tb40

Fig. 2(b)

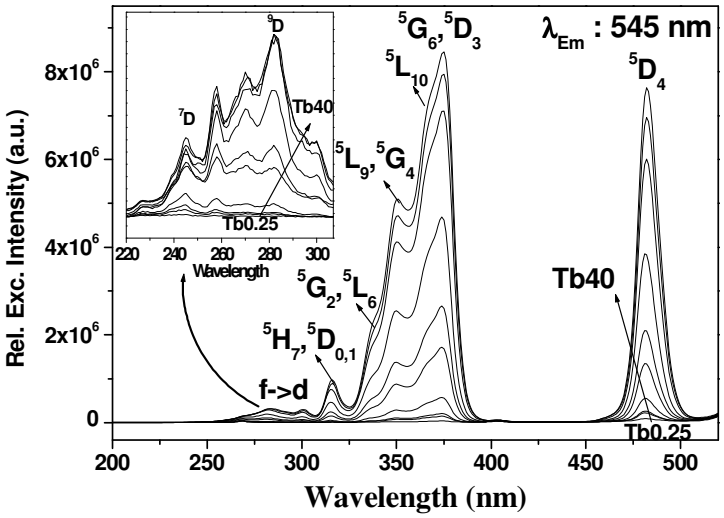
Rel. Exc. Intensity (a.u.)
Wavelength (nm)
λEm : 545 nm
5G6, 5D3
5L10
5D4
5L9, 5G4
5G2, 5L6
5H7, 5D0,1
f->d
Tb40
Tb0.25
9D
7D
Tb40
Tb0.25
Wavelength

Fig. 3

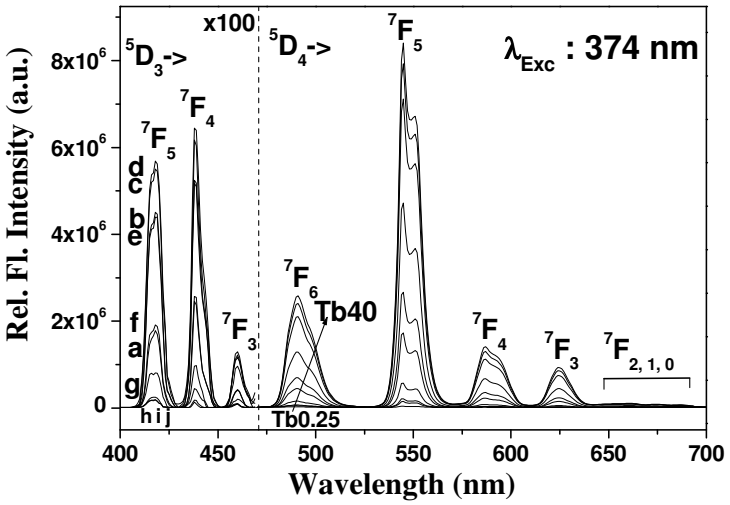
x100
$^5D_3$->
$^5D_4$->
$^7F_5$
λ_{Exc} : 374 nm
$^7F_4$
$^7F_5$
d
c
b
e
$^7F_6$
Tb40
f
a
$^7F_3$
$^7F_4$
$^7F_3$
$^7F_{2,1,0}$
g
h i j
Tb0.25
Rel. Fl. Intensity (a.u.)
8x10^6
6x10^6
4x10^6
2x10^6
0
400
450
500
550
600
650
700
Wavelength (nm)

Fig. 4

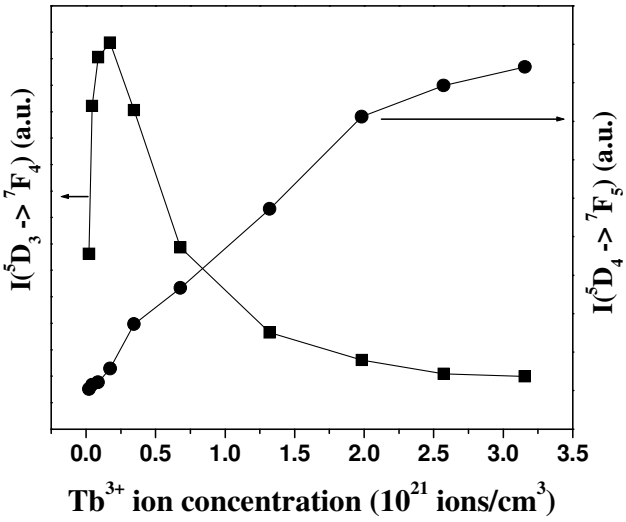
I(5D3 -> 7F4) (a.u.)
I(5D4 -> 7F5) (a.u.)
0.0
0.5
1.0
1.5
2.0
2.5
3.0
3.5
Tb3+ ion concentration (1021 ions/cm3)

Fig. 5

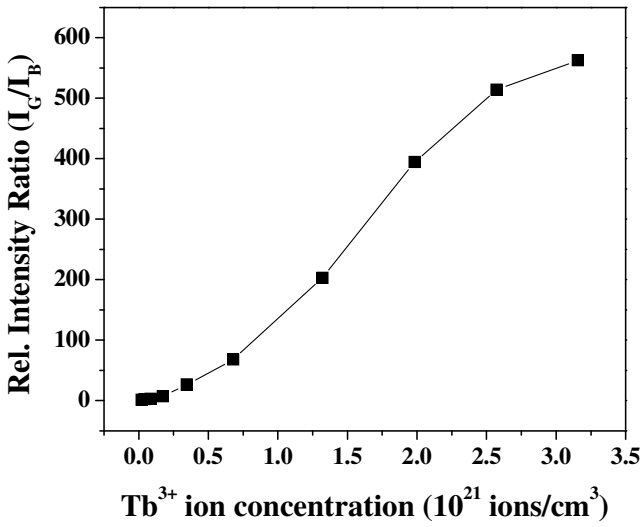
Rel. Intensity Ratio (I_G/I_B)
600
500
400
300
200
100
0
0.0
0.5
1.0
1.5
2.0
2.5
3.0
3.5
Tb^{3+} ion concentration (10^{21} ions/cm^3)

Fig. 6

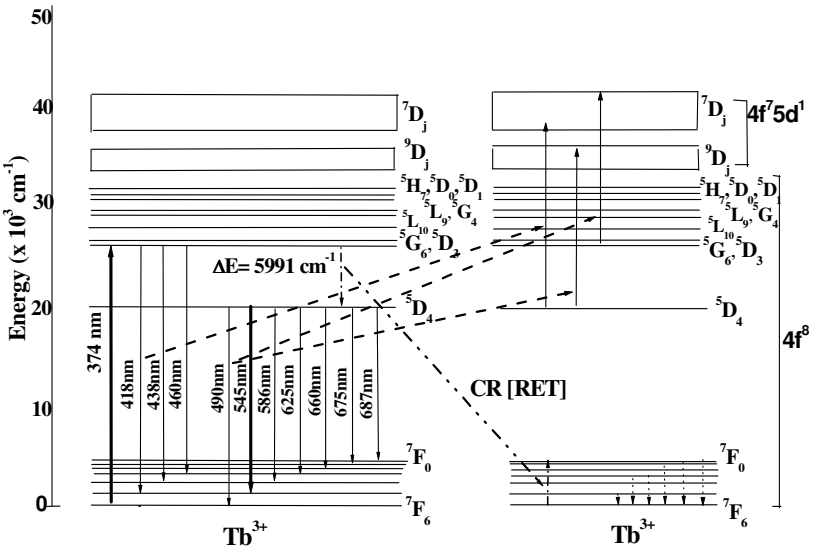
Energy (x 10^3 cm^{-1})
50
40
30
20
10
0
^7D_j
^9D_j
$^5H_7$,$^5D_0$,$^5D_1$
$^5L_9$,$^5G_4$
$^5L_{10}$,$^5G_6$,$^5D_2$
$^5D_4$
$^7F_0$
$^7F_6$
Tb^{3+}
ΔE= 5991 cm^{-1}
374 nm
418nm
438nm
460nm
490nm
545nm
586nm
625nm
660nm
675nm
687nm
CR [RET]
^7D_j
^9D_j
4f^{7}5d^1
$^5H_7$,$^5D_0$,$^5D_1$
$^5L_9$,$^5G_4$
$^5L_{10}$,$^5G_6$,$^5D_3$
$^5D_4$
4f^8
$^7F_0$
$^7F_6$
Tb^{3+}

Fig. 7

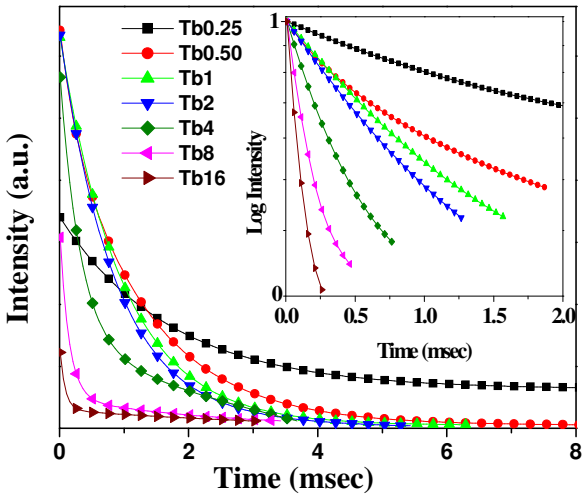
Tb0.25
Tb0.50
Tb1
Tb2
Tb4
Tb8
Tb16
Intensity (a.u.)
Time (msec)
Log Intensity
Time (msec)

Fig. 8

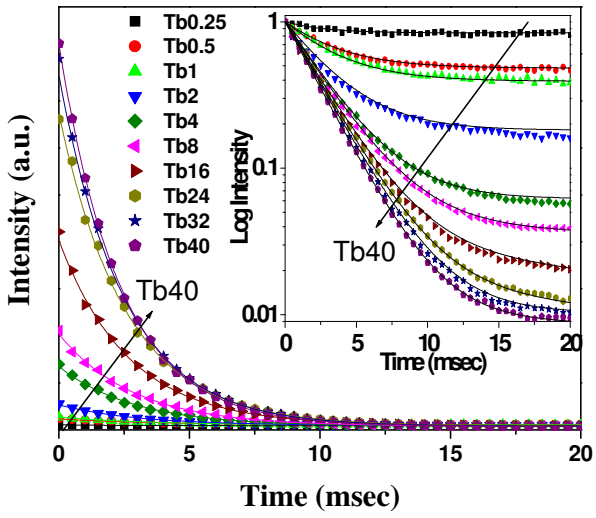
Tb0.25
Tb0.5
Tb1
Tb2
Tb4
Tb8
Tb16
Tb24
Tb32
Tb40
Tb40
Intensity (a.u.)
Time (msec)
0
5
10
15
20
Log Intensity
1
0.1
0.01
Tb40
Time (msec)

Fig. 9

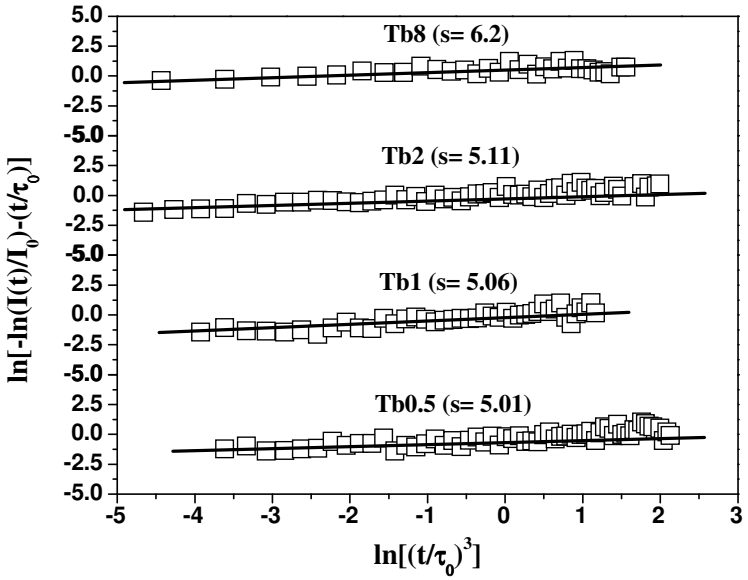

Fig. 10

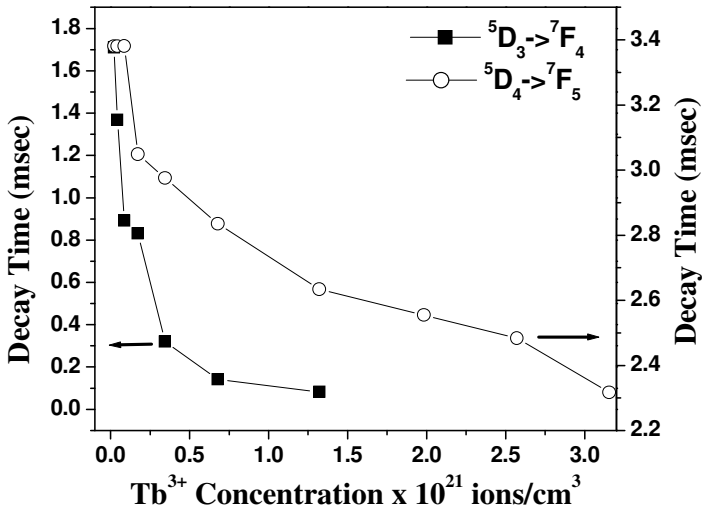
$^5D_3$->$^7F_4$
$^5D_4$->$^7F_5$
Decay Time (msec)
Decay Time (msec)
Tb^{3+} Concentration x 10^{21} ions/cm^3

Fig. 11